Materials Physics and Mechanics 20 (2014) 175-185 Received: April 29, 2014

SHOCK WAVE OVERPRESURE EVALUATION AT BLAST DETONATION INSIDE A DESTRUCTIBLE CONTAINER

M.V. Silnikov[1], A.I. Sadyrin[2], A.I. Mikhaylin[1*], A.V. Orlov[2]

[1]Institute of Military Engineering and Safety Research,

St. Petersburg State Polytechnical University, Polytekhnicheskaya 29, 195251, St. Petersburg, Russia

[2]Special Materials, Corp., St. Petersburg, Russia

*e-mail: mikhaylin@npo-sm.ru

Abstract. The article proposes a technique of blast-wave-pressure-express evaluation at a charge detonation inside a working space of the multi-camera container confined in an envelope filled with a multi-phase medium. The technique is based on a quasi-stationary symmetrical model of the container deformation. Calculated values of shock wave overpressures have been compared with experimentally obtained data for TNT charge detonations in the working space of various blast liquid inhibitors.

1. Introduction

Currently liquid blast inhibitors are widely used for mitigating dangerous effects caused by terrorist blasts [1, 2]. A liquid blast inhibitor is a multi-camera container confined within an elastic envelope filled with a liquid or multi-phase medium. The container design allows screening a bomb without touching it and provides safe isolation and destruction of the explosive due to the low probability of an accidental fuse detonation caused by a mechanical impact. It has been proved experimentally [3-6] that a blast shock wave resulted from an isolated high-explosive charge is much weaker than in case of the "open" charge detonation In real life it is often necessary to estimate a dangerous overpressure area by using blast inhibitor parameters and preliminary information on a bomb power. Therefore, models allowing estimating air-shock-wave pressure resulting from a charge detonation isolated by a container of that type are of interest.

A possibility of obtaining an accurate solution of the problem on deformation and destruction of an inhibitor for determining an air-shock-wave power by the full-scale numerical simulation method is limited, on the one hand, by complexity of the process, and, on the other hand, by impossibility to gain in practice the reliable estimate of the blast features, variations of existent and feasible inhibitors designs, asymmetry of the problem in actual practice, etc. However, it is acceptable to apply greatly simplified models for rough estimation of blast-shock-wave pressure.

The article proposes a technique of blast-wave-pressure-express-evaluation at a charge detonation inside a working space of a container. The technique is based on a quasi-stationary symmetrical model of the container deformation following by its instant destruction and formation of an air shock wave.

2. Validation of quasi-stationary model application

The process of high-explosive charge detonation inside an inhibitor that can be graphed as a spherical liquid layer can be conditionally divided into three stages. At the first and

the shortest stage the high-explosive detonation followed by expansion of the detonation products and shock wave formation occurs. The initial stage of the explosion (up to the moment when the shock wave reaches the wall of the inhibitor) does not depend on the inhibitor itself and is studied quite well. The duration of this stage is 20…40 μs. The air blast wave formation and propagation are illustrated by the diagram given in Fig. 1 [5].

The diagram reveals that the detonation products cause shock wave propagation through the air (AB curve). As this takes place, the blast products are separated from the air by a moving interface that is following the shock wave at the initial stages of the process development (AK curve).

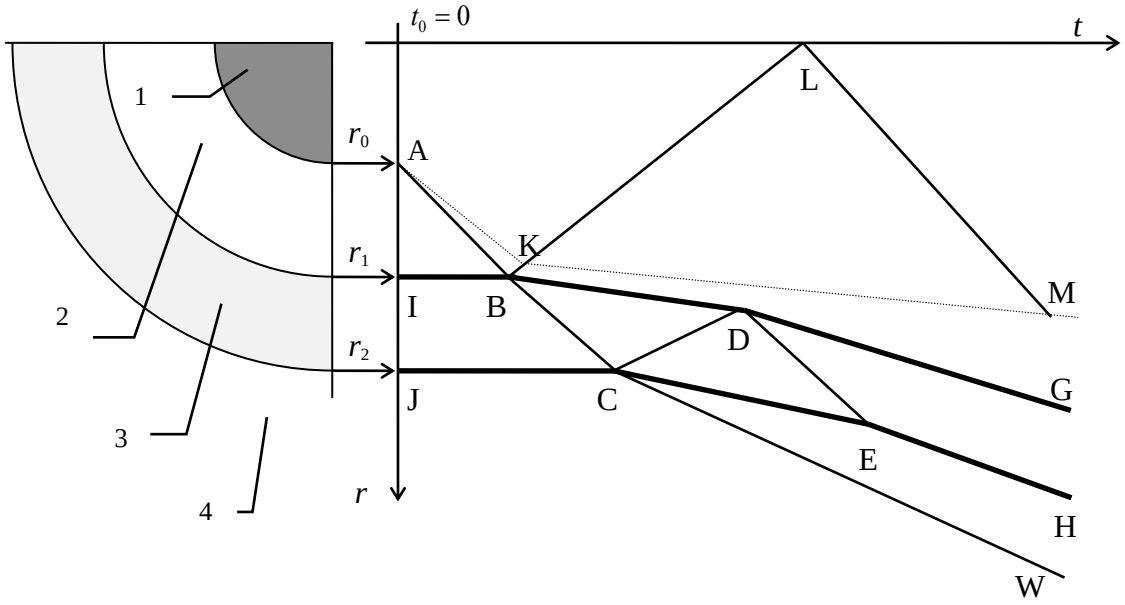

Fig. 1. *r–t* scheme: 1) high-explosive charge, 2) air working area, 3) liquid layer, 4) air space; AB, CW – fronts propagating through the air; SW; BC, DE – fronts propagating in the liquid; AKM – detonation products/air interface propagation trajectory; BK, KL, CD – reflected shock wave fronts propagating through the air, detonation products and the liquid correspondingly; IBDG, JCEH – inner and outer liquid layer surfaces trajectories correspondingly.

The second stage starts when the air shock wave reaches the inner surface of the liquid (point B), which results in the formation of a shock wave in the liquid (BC curve) and in a reflected shock wave in the air compressed by the detonation products (BK curve). The reflected shock wave is gradually passing into the detonation products and continuing its motion toward the symmetry center (KL curve). After its reflection from the symmetry center, the wave is moving through the detonation products (LM curve), then it is refracted at the air interface (point M) and within some time overtakes the liquid (point G). At a certain moment of time, the shock wave moving through the liquid reflects from the liquid's outer surface (point C), and, as a result, a pressure wave in the surrounding air (CW curve) is formed, a pressure-relieve wave is generated in the liquid (CD curve) and the outer surface of the liquid comes back to its initial velocity (CH curve). In the diagram, IBDG curve shows the change of the inner surface position, and JCH curve — the change of the liquid outer surface position.

This stage is characterized by comparative pressure equalization inside the air working area when, due to the reflection phenomenon, the shock wave runs several times between the walls of the liquid inhibitor and the air working area axis. This process is accompanied by the liquid motion inside the envelope either without its destruction or with few insignificant

ruptures. At the second stage some blast energy passes to the inhibitor. It can be shown that at the second stage several runs of the shock wave between the envelope and the symmetry axis are enough for getting the pressure equalization inside the air working area of the inhibitor.

The third stage starts at the moment when the envelope collapses and fast destruction of the liquid inhibitor occurs, which is accompanied by the liquid dispersion, the separation of drops and the final formation of the air shock wave. The container inner air working area radius is not more than 5-6 high-explosive charge radii, and the density of the medium filling the envelope is noticeably greater than both the shock wave air and detonation products densities behind the shock wave front. In view of the aforementioned facts, the first shock wave will be strong and its interaction with the container will not much differ from the interaction with a rigid surface.

Calculation of significant pressure impulse relaxation in a gas medium contained inside a rigid wall cylinder have revealed fast pressure equalization inside the liquid inhibitor air working area along the coordinate, in general during 4-5 runs of the shock wave between the wall and the working area axis. The testing using high-speed camera for recording the process [6] have proved that the envelope destruction starts within the time enough for 5-10 runs of the shock wave inside the air working area of the inhibitor. Thus, to a first approximation, the process of the further inhibitor destruction may be considered as a quasi-stationary process with the constant along the coordinate pressure inside the air working area.

3. Model of "bursting sphere"

Assume that the air working area expansion process continues from the initial radius r_1 to some limitary radius r_2 until the inhibitor destruction. When the destruction occurs, the detonation products start interacting with the atmosphere and a shock wave is formed. Mechanism of the shock wave formation differs from that given in the point blast theory. For the description of detonation products expansion following the inhibitor destruction a "bursting sphere" model was applied [7, 8]. The model is usually used for calculation of shock waves caused by a bursting pressurized vessel. A shock wave formed after the inhibitor destruction is weaker in comparison with a shock wave resulted from an open blast.

In "bursting sphere" model the shock wave pressure at the moment of the inhibitor envelope destruction is found from the equation for one-dimensional flow in a shock tube [9]:

$$\frac{P_1}{P_0}=\frac{P_{S0}}{P_0}\left[1-\frac{(\gamma-1)\frac{a_0}{a}\left(\frac{P_{S0}}{P_0}-1\right)}{\left(2\gamma_0\left(2\gamma_0+(\gamma_0+1)\left(\frac{P_{S0}}{P_0}-1\right)\right)\right)^{\frac{1}{2}}}\right]^{-\frac{2\gamma}{k-1}}, \qquad (1)$$

where P_1, P_0, P_{S0} - pressure in the air working area at the instant of the inhibitor destruction, atmosphere pressure, air shock wave front pressure, correspondingly; γ_0 and γ –the air and detonation products adiabatic values; a_0 and a – speed of sound in the air and in detonation products. Dimensionless pressure $\frac{P_{S0}}{P_0}$ or dimensionless overpressure $\overline{P}_{S0}=\frac{P_{S0}}{P_0}-1$ are found from (1) by the iteration method. In [8] the graphical results from (1) for various $\overline{P}_{S0}$ in the form of $(a/a_0)^2$ dependencies on P_1/P_0 are given. For finding the sought curve in the graphic and thereby $\overline{P}_{S0}$, it is necessary knowing pressure P_1 at the moment of the destruction and $(a/a_0)^2$ ratio. Pressure P_1 is found from the relief isentropic curve equation:

$P/\rho^{\gamma} = A.$ (2)

For typical high-explosives the ratio of specific heats for the detonation products during their expansion varies from $\gamma \approx 3$ to 1.2÷1.4. To take this effect into consideration, the method of representing the adiabat as two leg diagram offered in [10] is used

$P/v^{\gamma}{}_1 = A_1,\ P/v^{\gamma}{}_2 = A_2.$ (3)

The legs are conjugated at some point P_k, v_k, where P - pressure, $v=1/\rho$ -specific volume, A_1, A_2 – constants. The adiabatic conjunction point (3) for TNT of $\rho_0=1.62\cdot10^3$ kg/m^3 density is specified by $v_k=2.59\cdot10^{-3}$ m^3/kg and P_k = 1380 bar.
Thus, pressure P_1 is determined as

$P_1 = P_k(\rho_2/\rho_k)^{\gamma}.$ (4)

At the moment of the inhibitor destruction, density of the detonation products ρ_2 is determined from the mass conservation equation:

$m = 4/3\pi\rho_2 r_2^{\,3}.$ (5)

Here m is HE mass. The sound velocity in the detonation products determined by $a^2 = \left(\frac{\partial P}{\partial \rho}\right)_S$ at constant entropy and, taking into consideration the relief adiabatic equation (2), has the form:

$$a^2 = \frac{P_1}{\rho_2}\gamma\,. \tag{6}$$

Overpressure change dependence $\overline{P}_S$ on the distance shown in Fig. 2 is taken from [8]. The given graphic solution is the result of numerous calculations of bursting pressurized sphere performed with some assumptions. One of such assumptions is that the envelope effect was neglected. All calculation performed on the base of the ideal gas state equation.

The calculation results are given in Fig. 2 in dimensionless coordinates $\overline{P}_S$, $\overline{R}$. Dimensionless distance $\overline{R}$ is determined as:

$$\overline{R} = R\left[\frac{P_0}{E}\right]^{1/3}. \tag{7}$$

Dimensionless radius of the sphere at the moment of burst is

$$\overline{R}_2^{\,*} = r_2\left[\frac{P_0}{E}\right]^{1/3}, \tag{8}$$

where the gas energy in volume sphere V_2 under pressure P_1 is

$$E = \frac{P_1 - P_0}{\gamma - 1}V_2 = \frac{4\pi}{3}\frac{P_1 - P_0}{\gamma - 1}r_2^{\,3}. \tag{9}$$

Thus, the dimensionless sphere radius is

$$\overline{R}_2^{\,*} = \left[\frac{3(\gamma-1)}{4\pi\left(P_1/P_0 - 1\right)}\right]^{1/3}. \tag{10}$$

Figure 2 shows that, with the increase of the overpressure and the temperature inside and outside the liquid inhibitor at the moment of the collapse, $\overline{P}_S$ curves are getting closer to the curve characterizing the change of the overpressure resulted from the high-explosive charge detonation in the open. To determine the pressure/distance ratio for the blast sphere given parameters, it is necessary to find a point corresponding to dimensionless pressure $\overline{P}_{S0}$ and distance $\overline{R}^*$ at the moment of the liquid inhibitor collapse. Then, through the found point, the dependence curve $\overline{P}_S = \overline{P}(\overline{R})$ should be drawn equidistantly to two nearest curves.

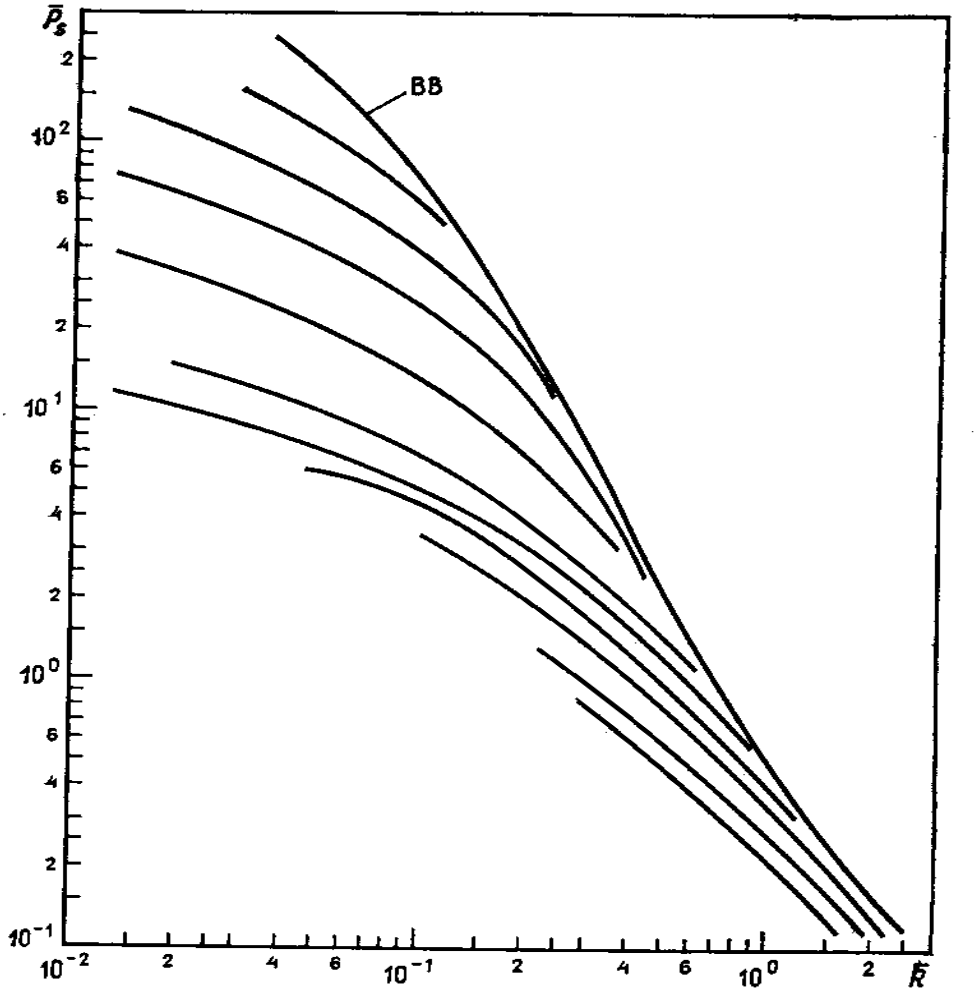

Fig. 2. Calculated relations $\overline{P}_S(\overline{R})$ for bursting spheres.

4. Modification of "bursting sphere" model

The calculated estimations performed according to the aforementioned diagram have revealed that in the range of the practical interest (30 – 100 kPa i.e. ear and lung injury threshold) the blast shock wave overpressure dependencies on non-dimensional distances (>0.7) for the sphere practically coincide with those for the open charge. Deviation is not more than 5 -10 %. Thus, at the sphere (inhibitor) blast and the open high-explosive charge detonation the same front shock wave overpressure values $\overline{P}$ are observed at the same distances $\overline{R}$ from the epicenter found from (7), where E – blast energy.

Consider the correlation between the distances from the epicenter to the equal shock wave pressure points at the open and isolated (simulated sphere blast) high-explosive charge

detonation. Assign «*i*» index to the sphere (inhibitor) and «*c*» index to the open high-explosive charge. Then $\overline{P}_c = \overline{P}_i$ if

$$\overline{R}_c = \overline{R}_i . \tag{11}$$

Assume that both open and isolated charges are spheres of the same high-explosive of density ρ_c and specific heat q_c. The charge inside the sphere has mass m_i and radius r_i, and those of the open charge – m_c and r_c. The sphere cavity is of radius r_{1c}. The sphere becomes deformed without destruction up to r_{2c} radius. High-explosive blast energy can be found as

$$E_c = m_c q_c = 4\pi/3\ \rho_c q_c r_c^3 . \tag{12}$$

The sphere blast energy is

$$E_i = \frac{P_1 - P_0}{\gamma - 1} V_{2i} \approx \frac{4\pi}{3} \frac{P_1}{\gamma - 1} r_{2i}^{\ 3} . \tag{13}$$

P_0 can be neglected in comparison with the sphere cavity pressure P_1 at the moment of sphere destruction, when P_1 two orders exceed P_0. P_1 is expressed in terms of the adiabatic equation taking into consideration the conjugation method (4), where ρ_2 is the density of the detonation products filling the sphere cavity V_{2i} at the detonation of the high-explosive charge of radius r_i.

$$\rho_2 = \rho_c (r_i / r_{2i})^3 , \tag{14}$$

$$V_{2i} = 4\pi/3\ r_{2i}^3 . \tag{15}$$

From equations (7, 11-15) one obtains:

$$\frac{R_i}{R_c} = A \frac{r_{2i}}{r_c} \left(\frac{r_i}{r_{2i}} \right)^{\gamma} , \tag{16}$$

where $A = \left[\frac{P_k \rho_c^{(\gamma-1)}}{(\gamma-1) q_c \rho_k^{\ \gamma}} \right]$ is the constant for a particular high-explosive.

For detonation of the open and isolated charge of the same radius r_i we have

$$\frac{R_i}{R_c} = A \left(\frac{r_i}{r_{2i}} \right)^{(\gamma-1)} . \tag{17}$$

This equation allows to compare the distance from the charge to a point of the given front shock wave pressure at the detonation of high-explosive charge of radius r_e isolated by a sphere of radius r_{1c}, and an envelope withstanding ultimate elongation r_{2c}/r_{1c} with the distance to the same shock wave pressure point at the open charge detonation.

For particular high-explosive, R_c/r_c ratio is a non-dimensional parameter determining the front shock wave pressure. From (16)

$$\frac{R_c}{r_c} = \frac{1}{A} \frac{R_i}{r_{2i}} \left(\frac{r_{2i}}{r_i} \right)^{\gamma} . \tag{18}$$

Thus at high-explosive charge detonation inside the inhibitor working area $\frac{1}{A} \frac{R_i}{r_{2i}} \left(\frac{r_{2i}}{r_i} \right)^{\gamma}$ or

$\frac{n}{A}\frac{R_i}{r_{1i}}\left(\frac{r_{2i}}{r_i}\right)^{\gamma}$ is the dimensionless parameter determining the pressure, where $n=\frac{r_{2i}}{r_{1i}}$ is the envelope ultimate elongation. Inserting this parameter into one of the known *P(R)* dependencies obtained with the testing data approximation, we can perform an evaluative prognosis of the pressure reduction at various distances from the epicenter resulted from the inhibitor application.

5. Testing technique

The following tests have been performed to determine a shock wave pressure at different distances from a high-explosive charge of various mass isolated by various type inhibitors. The 0.1, 0.42 and 1.0 kg TNT blasts were conducted on a rigid surface (steel plate). The shock wave pressure was recorded by 6-12 piezoelectric pressure sensors placed along two perpendicular lines at 0.8 - 4.0 m from the charge. For 0.1-kg TNT charge detonation the sensors were placed 0.1m above the ground, for 0.42 and 1,0 kg charges – at 0.5 – 1.5 m above the ground.

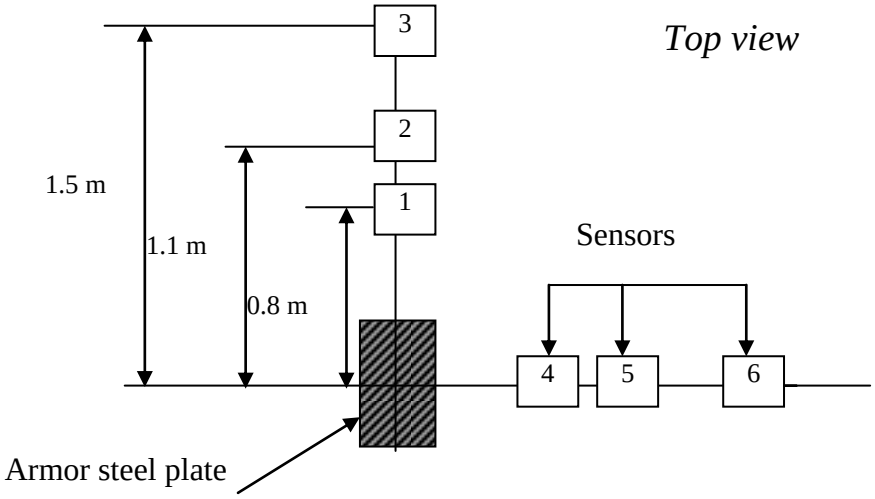

Fig. 3. Layout of pressure sensors.

The pressure sensors were calibrated with a dynamic method; the pressure transformer was subjected to blast waves of a given intensity, resulting from 140 g spherical 50/50TNT-RDX charges.

Samples of inhibitors of five types were used in the testing (Table 1). For the tests with 0.1-kg TNT, cylinder shape inhibitors with the top section were made. Hollow walls of the cylinder and those of section formed a single volume. The sample cross section is graphed in Fig. 4. The elastic envelope was made of 2 mm polyethylene. The working space dimensions (3 in Figю 4) of the samples type1 and type 2 were identical: height 0.15 m and diameter 0.15 m. Thus the equivalent volume sphere radius is 0.086 m (Table 1). The density of the working medium and, therefore, the weight of the inhibitor were varied. For isolating 0.42 kg charge, two types of inhibitors (3 and 4, Table 1) with different volume and shape of the working space, envelope (rubber or polyurethane), weight (10 or 19 kg), but with the same working medium were used. 1-kg TNT charges were isolated by multi-camera containers with rubber envelopes with equivalent radius of the working space of 0.201 m (type 5). Water solution of calcium chloride (density $1.29\cdot10^3$ kg/m^3) –sample No2, and ethylene glycol (density $0.96\cdot10^3$ kg/m^3) – the other samples, were used as the working liquid. HE charge was covered with the inhibitor in such a way as to be on the axis of the inhibitor symmetry.

Table 1. Parameters of blast inhibitor samples.

Sample No	HE weight (m), kg	Sample weight (M), kg	Equivalent sphere radius (R_S), m
1	0.1	5.6	0.086
2	0.1	7.1	0.086
3	0.42	10	0.090
4	0.42	19	0.138
5	1.0	53	0.201

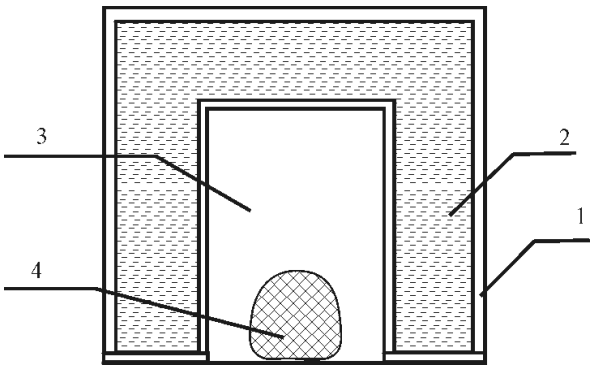

Fig. 4. Scheme of the blast inhibitor cross section: 1) elastic envelope, 2) liquid-gas medium, 3) working space, 4) HE charge.

Efficiency of the pressure measuring system was verified by conducting detonations of the open high-explosive charges (0.1, 0.42 and 1.0 kg.).The recorded blast overpressure data agreed with the data found from the Sadovskiy empirical formula for blasts on the rigid surface with accuracy $\pm$12% [9]

$$P_* = 0{,}95/R_* + 3{,}9/R_*^2 + 13/R_*^3, \quad (19)$$

where P_*: $= P/P_0$, $R_* = R/m^{1/3}$, P – front shock wave overpressure, P_0 –air pressure, R – distance from the pressure point to the blast epicenter, m – HE charge weight; or in dimensionless distance terms $R_{dl} = R/R_0$ for trotyl of 1.62 10^3 kg/m^3 density:

$$P_* = 17{,}9/R_{dl} + 1390/R_{dl}^2 + 87200/R_{dl}^3. \quad (20)$$

6. Discussion of the results obtained

Calculated values of shock wave overpressures have been compared with experimentally obtained data for TNT charge detonations in the working space of various blast liquid inhibitors. Modified model of "bursting sphere" allowed greatly simplifying calculation of evaluated values. Using Table 1 data, the calculation has been conducted by substituting (18) into empirical dependence $P(R)$ (20) for the open-air blast. The ratio of specific heats of detonation products has been assumed as $\gamma \approx 1.33$.

Figures 5-7 present examples of front shock wave overpressure versus the distance from the epicenter of the charges. The charges detonated are 0.1 kg TNT (inhibitors of type 1 and type 2 with different medium, but the same working space volume), 0.42 kg TNT (two types of inhibitors 3 and 4 with various working space volumes) and 1 kg TNT (inhibitors of type 5). A comparison of the diagrams constructed based on the calculated results and the approximated experimental data obtained shows that in spite of the simplicity of the model it allows performing express evaluation of pressure resulted from the high-explosive detonation isolated by the container filled with the liquid.

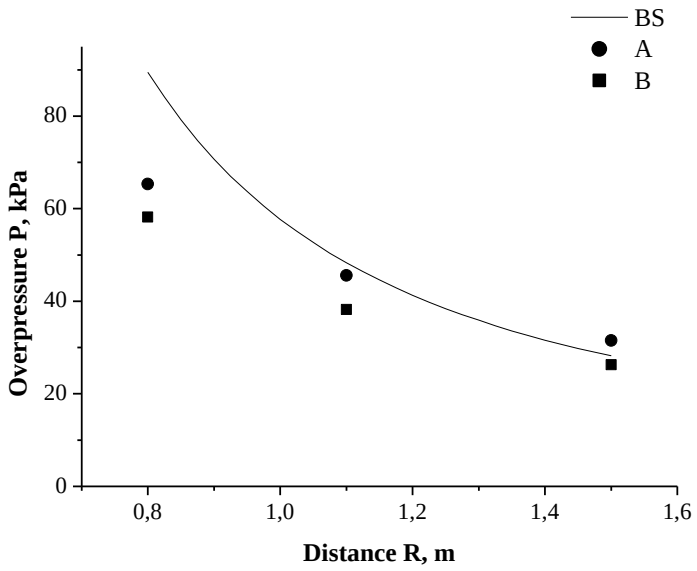

Fig. 5. Front shock wave overpressure caused by isolated 0.1-kg TNT charge; BS curve – results calculated with the modified model of 'explosive spheres" for 0.086 m radius sphere; A and B dots correspond to experimental data obtained for 1 and 2 types of inhibitors (Table 1).

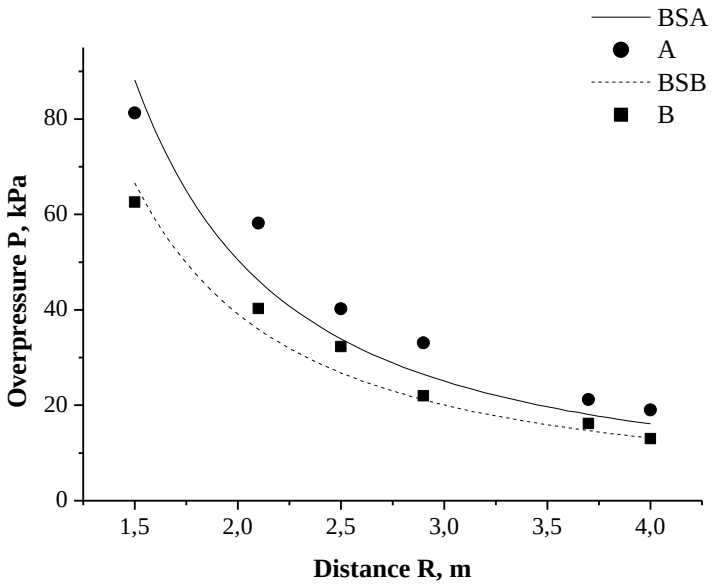

Fig. 6. Front shock wave overpressure resulted from the isolated 0.42 kg TNT: BSA and BSB curves– results calculated with the modified model of 'explosive spheres" for 0.09 and 0.138 m radius spheres; A and B – experimental data obtained for 3 and 4 types of inhibitors (Table 1).

Figure 8 presents a correlation between the shock wave overpressure caused by 1-kg TNT open charge detonation (to formula (20)) and 0.201-m radius sphere (to modified model of "bursting sphere") at various distances from the epicenter. Pressure level 100 kPa is the lung hemorrhage threshold. Data given in Fig. 8 show the reduction of the dangerous zone radius from 3.3-m to 1.5-m as a result of the blast isolation. As this takes place, degree of the shock wave overpressure mitigation is increasing with the approaching to the epicenter, i.e. in the most dangerous zone.

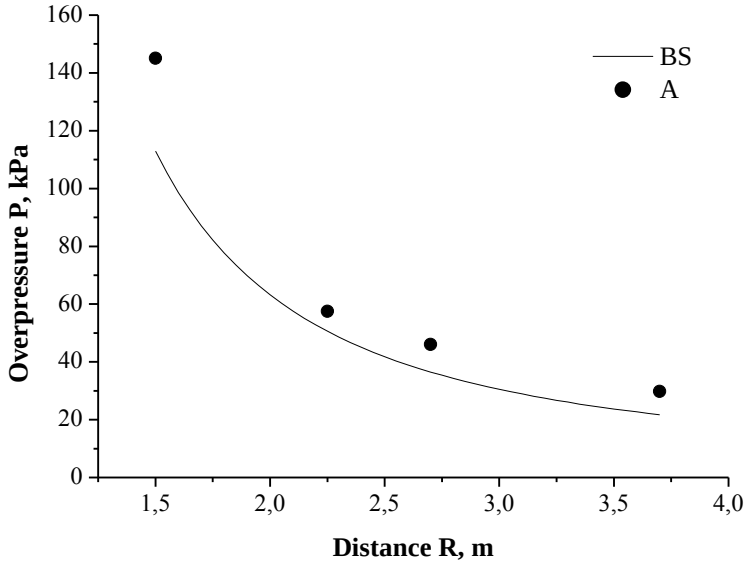

Fig. 7. Front shock wave overpressure caused by isolated 1 kg TNT detonation: BS curve – results calculated with the modified model of 'explosive spheres" for 0.201-m radius sphere; dots – experimental data obtained for inhibitors of type 5 (Table 1).

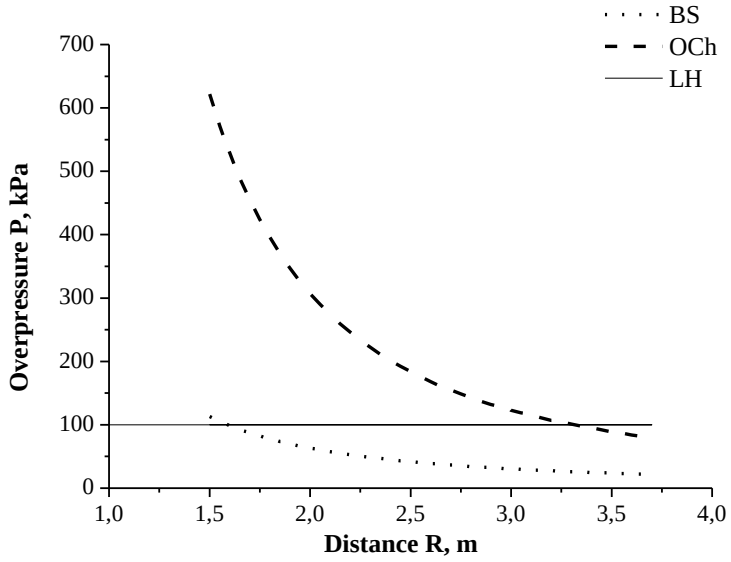

Fig. 8. Front shock wave overpressure caused by 1 kg TNT detonation BS curve – results calculated with the modified model of 'explosive spheres" for 0.201 m radius sphere; OCh curve – results calculated by formula (20) for an open charge; Pressure level 100 kPa shows the dangerous for human health zone.

It should be stressed out again that approximation of the modified model of "bursting sphere" is acceptable only if the pressure is determined in that $\overline{P}_S(\overline{R}\ )$ area (Fig. 2) where the dependencies for bursting sphere are the closest to the dependencies for the open high-explosive. At the same time, evaluations performed to the "bursting sphere" model shows that it is exactly in this area $\overline{P}_S(\overline{R}\ )$ lies the practical interest when determining the safe zone. It is explained by two factors:

- Values of the following parameters, viz: inhibitor working space volume/high explosive

charge power ratio determining $\overline{P}_{S0}$ and $\overline{R}_2^*$ at the moment of detonation,

- Pressure level safe for human life ($\overline{P}_S \leq 0.3 \ldots 1.0$), that can be achieved at distance $\overline{R} \geq 0.7$.

Simulating the inhibitor blast deformation demonstrates that shock wave action makes the process significantly non-stationary that causes various kinds of instabilities. Development of the instabilities causes the inhibitor destruction at the earlier stage than in case of the quasi-stationary model. Analysis of the inhibitor envelopes destroyed by the blast also testifies that before the destruction no final pressure balance inside the working space of the inhibitor occurs. As a consequence, physical-mechanical properties of the dispersion medium as a medium of shock wave propagation play an important role in the process of the inhibitor destruction. Such properties determine the extent to which the liquid inhibitor protective characteristics may decrease in comparison with the "ideal" model. Nevertheless, the practical usage of the proposed model seems to be grounded and allows getting correct evaluations of blast waves parameters for various conditions of blast inhibitors applications.

References

[1] M. Silnikov, A. Mikhailin, N. Vasiliev, V. Ermolaev, V. Shishkin, In: *Detection and Disposal of Improvised Explosives*. NATO Seminar Proceedings (Springer Verlag, 2006), p. 97.
[2] B.E. Gelfand, M.V. Silnikov, M.V. Chernyshov // *Shock Waves* **20** (2010) 317.
[3] B.E. Gelfand, M.V. Silnikov // *Journal Physique* **12** (2002) Pr 7/371.
[4] B.E. Gelfand, M.V. Silnikov, A.I. Mikhailin, A.V. Orlov // *Combustion, Explosion and Shock Waves* **37** (2001) 607.
[5] K. Kailasanath, P.A. Tatem, J. Mawhinney // *Naval Research Laboratory Report*, 2002, NRL/MR/6410-02-8606 .
[6] M.V. Silnikov, A.I. Mikhaylin // *Acta Astronautica* **57** (2014) 30.
[7] A. Adamczyk, R.A. Strehlow, *Terminal energy distribution of blast waves from bursting spheres* (NASA contractor report; NASA CR-2903, 1977).
[8] W.E. Baker, P.A. Cox, P.S. Westine, J.J. Kulesz, R.A. Strehlow, *Explosion Hazards and Evaluation* (Fundamental Studies in Engineering 5, Elsevier Scientific Publishing, 1983).
[9] M.A. Sadovskiy, *Selected Works: Geophysics and Physics of Explosion* (Nauka, Moscow, 2004).